Appendix A. *Supplementary Material*

Antarctic regions

We initially localize over all of Antarctica, and analyze the mass change with a truncated basis consisting of 100 Slepian functions. Antarctica is large enough to be subdivided into smaller regions that have enough well-concentrated basis functions (at a bandwidth $L = 60$) to solve for the changes in the spatial pattern over time. We chose five regions based on the general trends seen in the analysis over the whole continent (Fig. 1): the West Antarctica Ice Sheet (16 functions), the Antarctic Peninsula (5 functions), the coastal region around Dronning Maud Land (20 functions), the coastal region around Wilkes Land (26 functions), and an interior region around the South Pole (34 functions). These regions were initially created using drainage-system basin outlines of grounded ice from ICESat altimetry data (Zwally et al., 2012). For basins in the Antarctic Peninsula, outlines including floating ice were used, otherwise this area was not large enough to yield a reasonable number of well-concentrated Slepian functions. For the interior basin referred to as Basin 3 by Zwally et al. (2012), elevations below 2500 m were included in the region for Dronning Maud Land, while higher elevations were included in the interior region.

These five regions share common boundaries where they are adjacent over land. A buffer region is used only on the land-ocean boundary of each region to account for mass changes near the coast. This construction ensures that from the perspective of Slepian functions, the regional functions are orthogonal. That is, the localization kernels for the regions can be summed to form the equivalent kernel used for Antarctica as a whole. Hence, differences in the trends between the regions and the whole (see Table S1) are due to rounding and statistical effects, not to double-counting. To calculate the mass change for the whole East Antarctic Ice Sheet, as reported by other groups, one needs to sum the estimates from the Dronning Maud Land, Wilkes Land, and East Antarctic Interior regions (i.e. +56 Gt/yr for the IJ05_R2 GIA model).

Region	IJ05_R2	W12a_v1	Range
West Antarctic Ice Sheet	−121 ± 8	−132 ± 8	−140 to −113
Antarctic Peninsula	−27 ± 2	−27 ± 2	−29 to −25
Dronning Maud Land	+62 ± 4	+73 ± 4	+58 to +77
Wilkes Land	−17 ± 4	−10 ± 4	−21 to −6
East Antarctic Interior	+11 ± 3	+22 ± 3	+8 to +25
Direct sum of five regions	−92	−74	
Continent-wide analysis	−92 ± 10	−73 ± 10	−102 to −63

Table S1: Ice mass balance trend estimates, and their 2σ confidence region, of the various regions in gigatons per year (Gt/yr) for two GIA models. The final column shows the range of estimates spanned by changing the GIA model and accounting for mass estimation uncertainty.

Supplementary discussion

In Fig. S4 (top row) we show the mass change from a localization of the Center for Space Research (CSR) RL–05 solutions over the whole of Antarctica, using the alternate GIA correction models IJ05_R2 (as in the Main Text) and W12a_v1. In the past decade, differences between GIA models for Antarctica have diminished (King, 2013). While different GIA models still alter the mass loss trends by more than the uncertainty implied by the data themselves, the changes that arise in the recovered spatial pattern of the ice mass change from using different GIA models are relatively small compared to the mass balance signal.

In Fig. S4 (bottom row), we show the ice mass changes using both GIA models but using the RL–05a monthly solutions from the GeoForschungsZentrum (GFZ). The differences between the models derived from the different data centers are of the same order as the changes that originate from switching GIA models. We note that the solutions derived from GFZ data are more spatially variable than those derived from CSR data. The effect is most apparent in the Wilkes Land region, and generally results in somewhat larger uncertainties when estimating the trends.

The changes in the mass trends for each region under either GIA model can be seen in Fig. S5. Our fitted trends do not include the uncertainty on the GIA model corrections themselves, but a total range, including the fit uncertainty and model differences is reported in Table S1.

The maps of yearly mass change for West Antarctica (Fig. S6) include the intervening years not shown in Fig. 3, and confirm that changes between individual years are gradual. Each panel for a specific year (e.g., 2003) shows the changes during that calendar year, occurring between January of the labeled year and January of the next (e.g., January 2003 to January 2004). We show similar yearly results for the Antarctica Peninsula (Fig. S7), the Dronning Maud region (Fig. S8), and the Wilkes Land region (Fig. S9).

Over the past decade, in the Antarctic Peninsula (Fig. S7), mass loss has increased in Palmer Land (the southern half of the Peninsula), leading to an overall increase in the mass trend over time. In the Dronning Maud region of East Antarctica (Fig. S8), the increase in mass gain along the coast is easily seen, however, since the fitted functions vary smoothly with time, the sharp change in time observed in the data is not expressed in this figure. Years 2003 and 2004 exhibit north-south striping which is unlikely to be real mass change signal. In this region, GRACE data from 2003 and 2004 have a variance several times higher than during the rest of the time period, and the estimates for this time interval cannot be considered accurate. In Wilkes Land (Fig. S9), consistent areas of mass loss near the Totten (~115°E) and Cook basins (~150°E) correspond to mass losses seen in other GRACE studies.

Overall, the mass changes observed in regions other than West Antarctica are of lower magnitude and closer to the noise threshold. Consequently they should be interpreted cautiously.

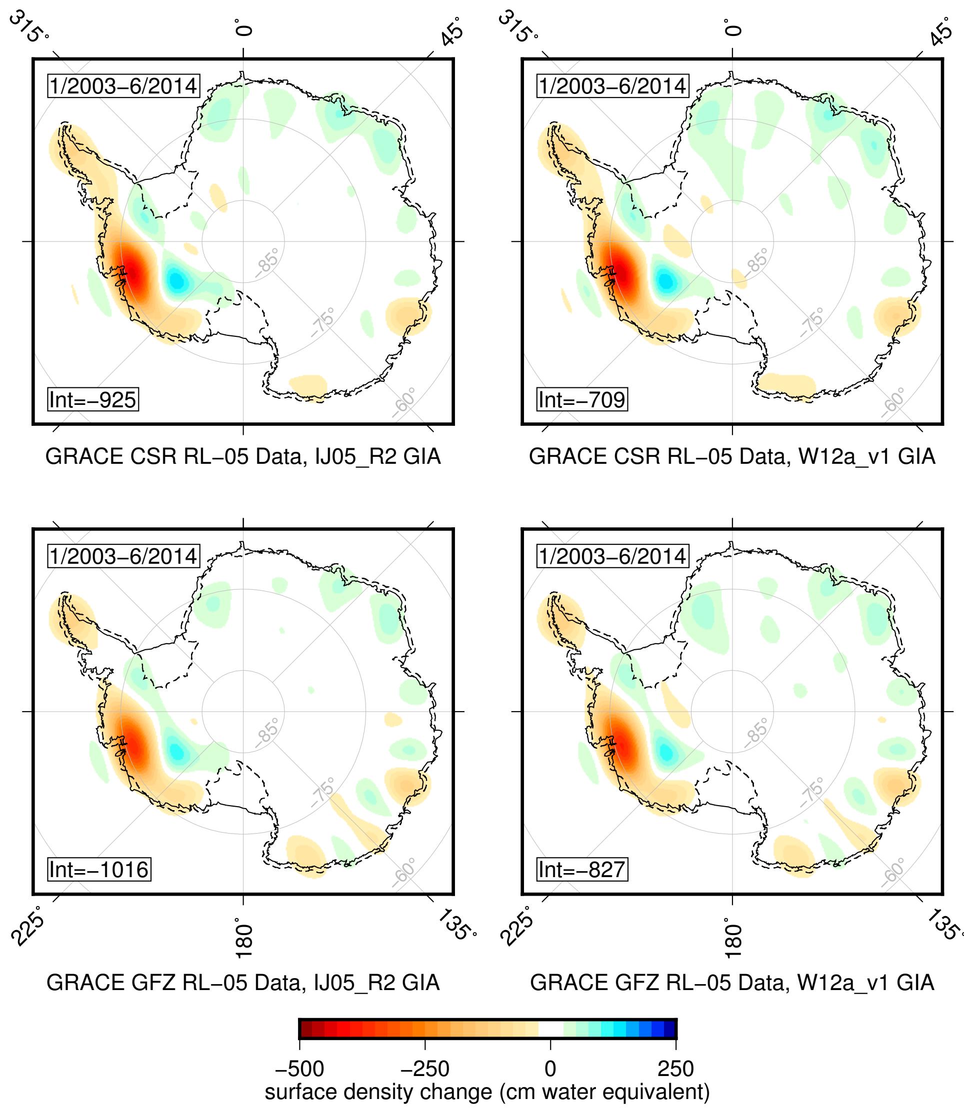

Figure S4: Ice mass change over Antarctica for the time period January 2003 to June 2014. These estimates derive from localization over the whole of Antarctica. The top row uses CSR RL–05 data, while the bottom row uses data from GFZ RL–05a. The solutions in the left column are corrected using the GIA model IJ05_R2 (Ivins et al., 2013). The solutions in the right column are corrected using the GIA model W12a_v1 (Whitehouse et al., 2012).

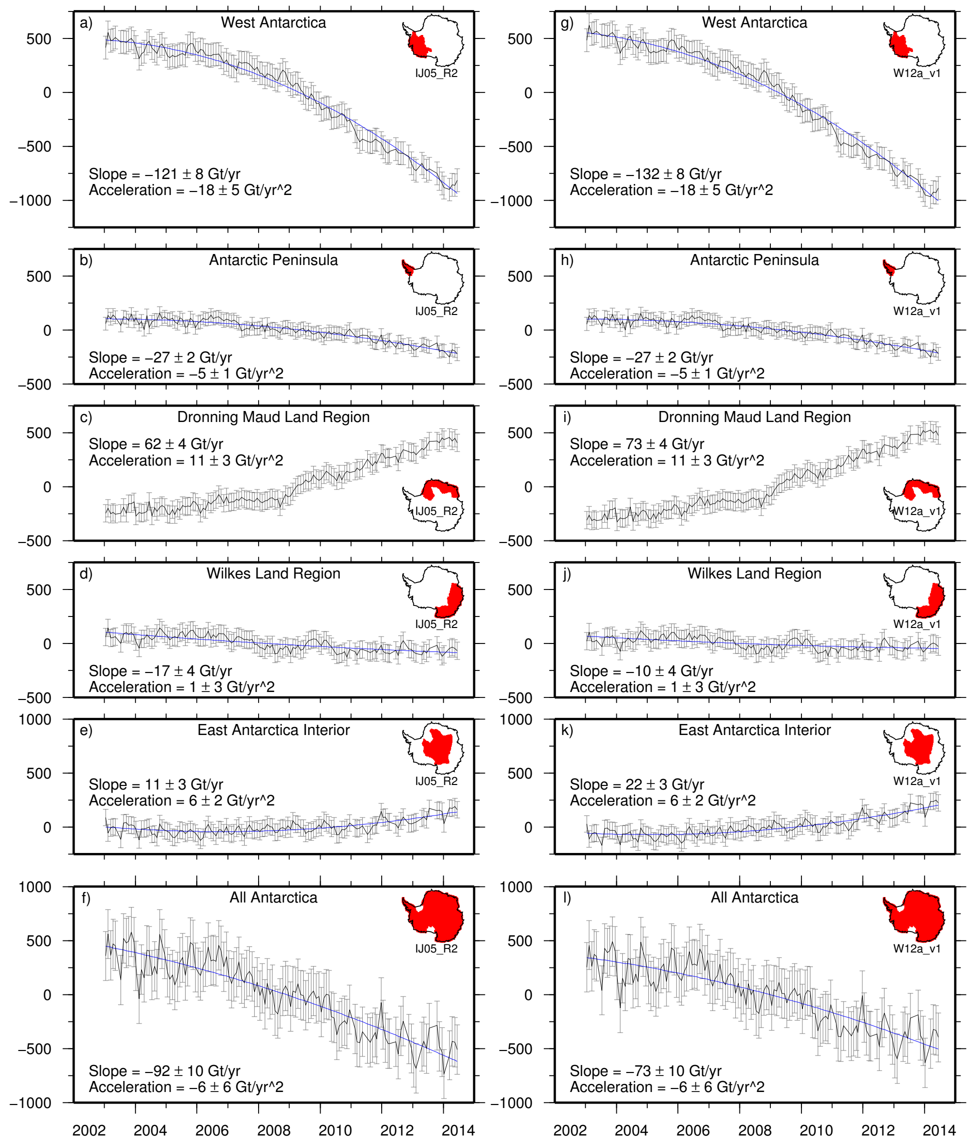

Figure S5: Ice mass trends corrected for the IJ05_R2 (Ivins et al., 2013) GIA model (left) and for the W12a_v1 (Whitehouse et al., 2012) GIA model (right), in gigatons, for several regions of Antarctica, as labeled. The regions covered by each localization are shown in red in the top right of each graph. The black lines are monthly GRACE observations with gray 2σ error bars determined from our analysis. The solid blue lines are the best-fit quadratic curves.

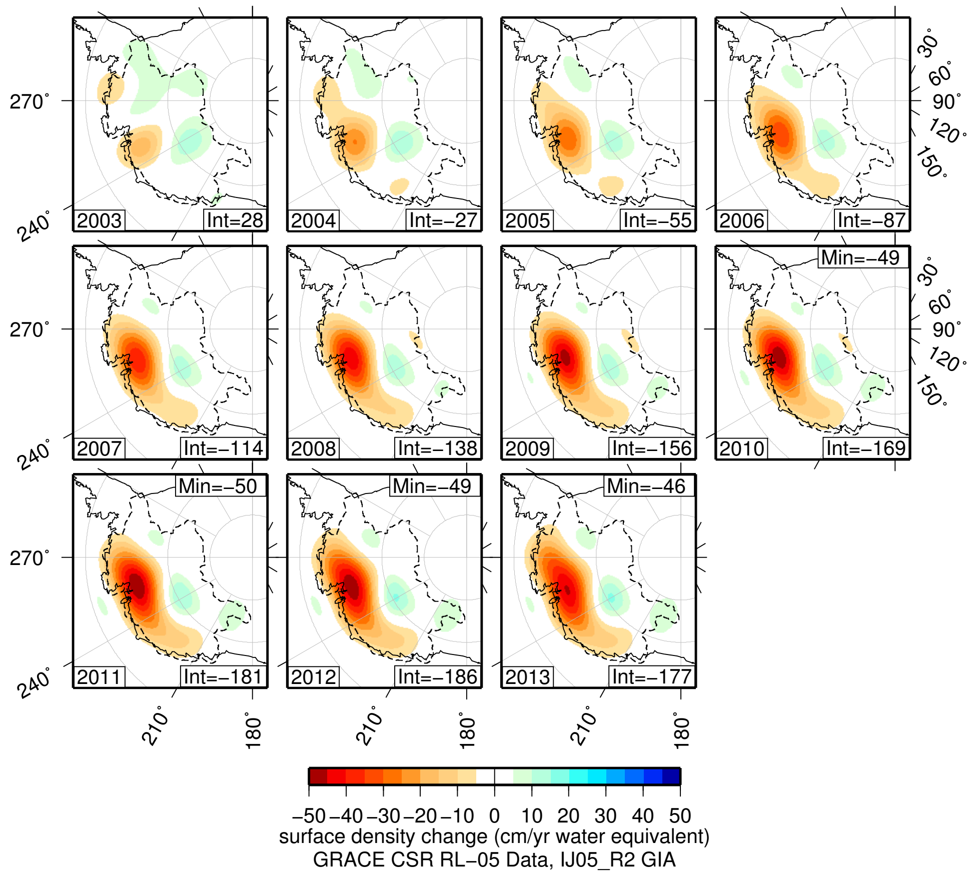

Figure S6: Yearly-resolved maps of ice mass change (mass corrected using the Ivins et al., 2013, model) over West Antarctica, from the beginning of 2003 to the beginning of 2014. Each panel shows the mass changes during the labeled calendar year, covering the difference of the signal estimated between January of that year and January of the next. For example, the first box shows the mass change from January 2003 to January 2004. Changes seen between the years are thus accelerations. The area of each panel corresponds to the area of box a in Fig. 1. The area of the localization includes grounded ice in West Antarctic basins with a 0.5° buffer towards the ocean, and is outlined with a dashed line. The solid black line is a coastline including ice fronts. The integral values (over the region) of the mass change per year are shown as “Int”, expressed in gigatons (Gt). When the color bar is near saturated, as in years 2010–2013, the minimum value of the field is shown in the top right as “Min” with units of centimeters per year water equivalent.

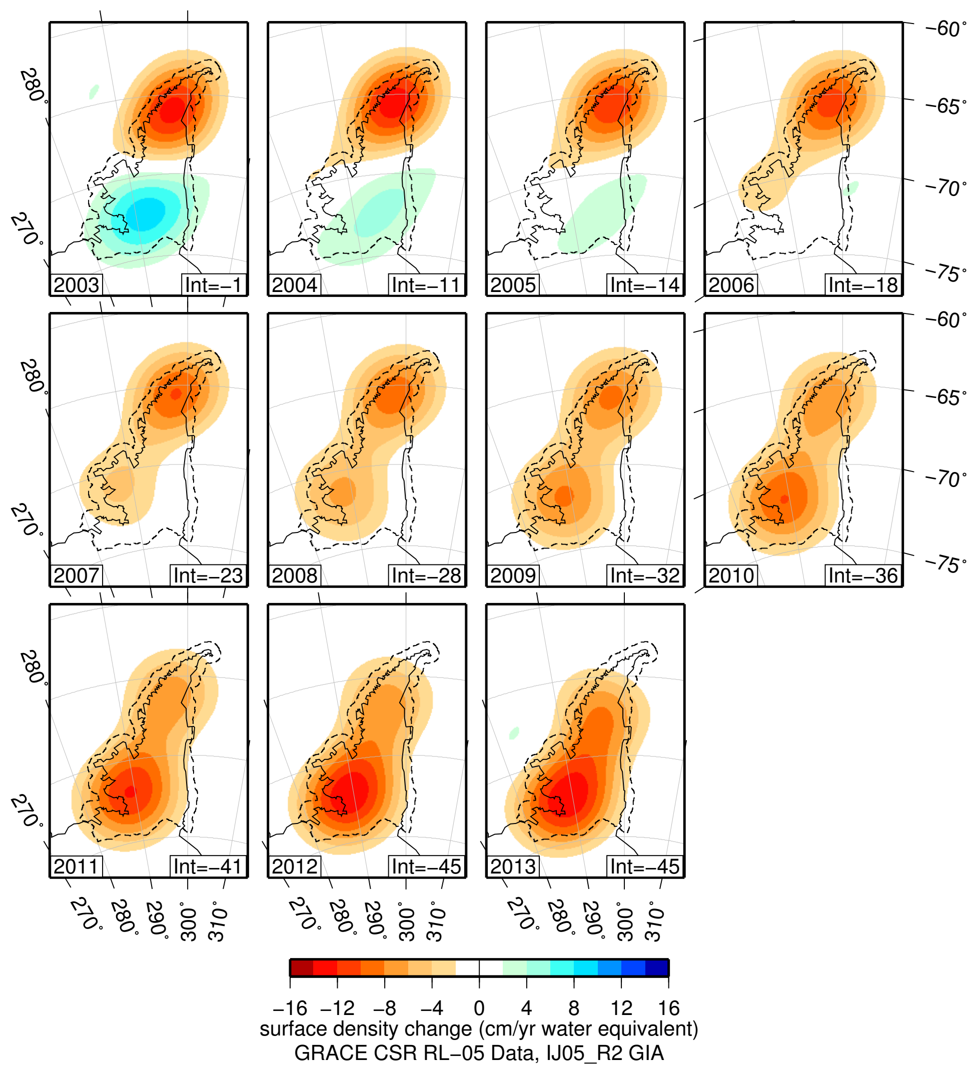

Figure S7: Yearly-resolved maps of ice mass change (mass corrected using the Ivins et al., 2013, model) over the Antarctic Peninsula, from the beginning of 2003 to the beginning of 2014, in a layout as in Fig. S6. The area of each panel corresponds to the area of box b in Fig. 1.

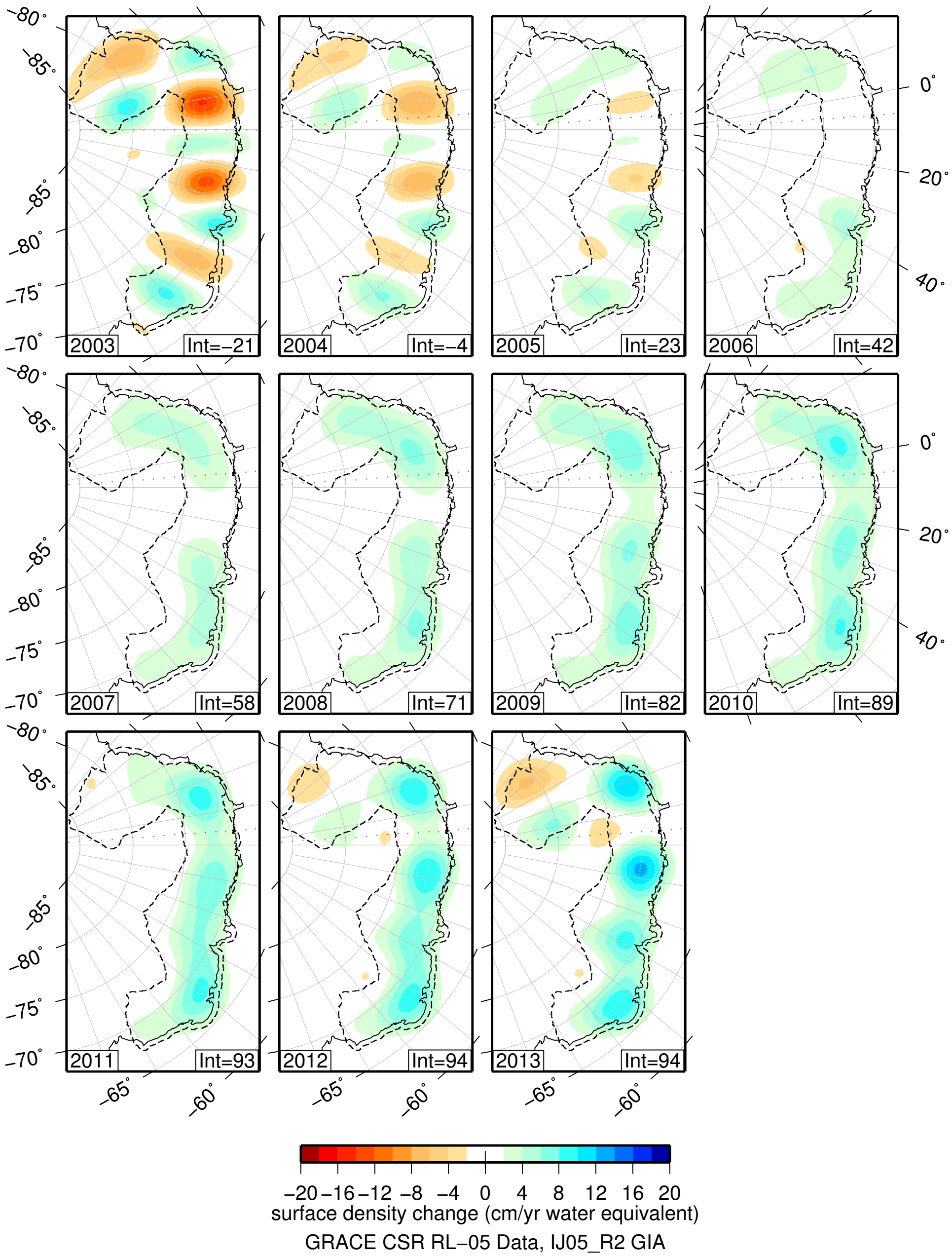

Figure S8: Yearly-resolved maps of ice mass change (mass corrected using the Ivins et al., 2013, model) over the Dronning Maud Land region, from the beginning of 2003 to the beginning of 2014, in a layout as in Fig. S6. The area of each panel corresponds to the area of box c in Fig. 1.

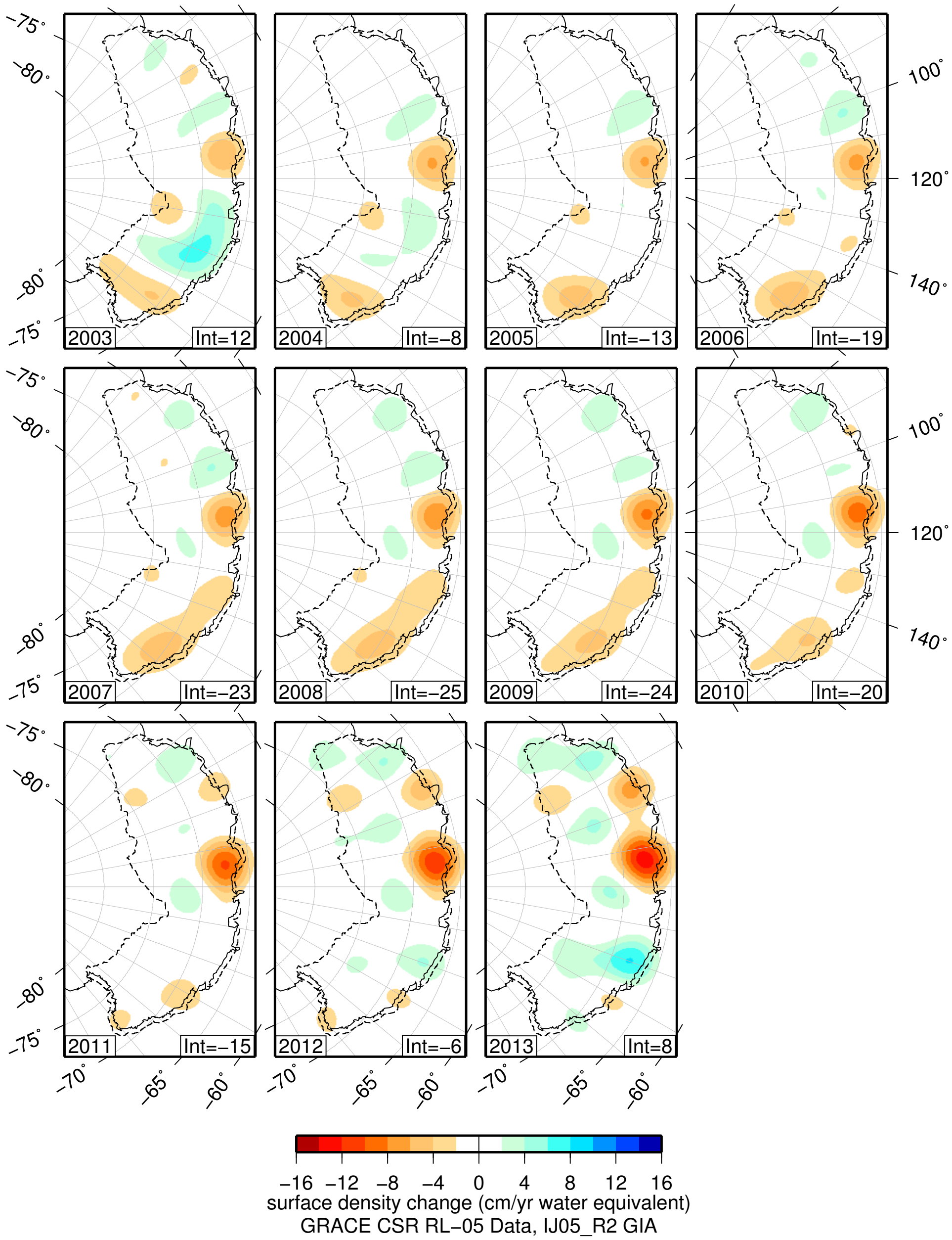

Figure S9: Yearly-resolved maps of ice mass change (mass corrected using the Ivins et al., 2013, model) over the Wilkes Land region, from the beginning of 2003 to the beginning of 2014, in a layout as in Fig. S6.